Isothermal crystallization of isotactic polypropylene in dotriacontane. IV. Effect of dilution and crystallization temperature on overall crystallization kinetics

Yu. F. Wang* and Douglas R. Lloyd†
Department of Chemical Engineering, Center for Polymer Research, The University of Texas at Austin, Austin, TX 78712, USA
(Received 10 August 1992; revised 24 February 1993)

The overall isothermal crystallization kinetics for isotactic polypropylene (iPP) in dotriacontane was investigated. Half-time was determined via differential scanning calorimetry as a function of the experimentally-controlled variables, dilution and crystallization temperature. Polymer concentration was varied from 100 to 10 wt% iPP in 10 wt% intervals. Crystallization temperature was varied from 415 to 380 K in 1 K intervals. The influence of these variables on crystallization mechanism and spherulitic structure, as implied by the Avrami analysis, was determined, and their influence on fold surface energy was exained by the Lauritzen and Hoffman analysis.

(Keywords: crystallization; isotactic polypropylene; kinetics)

INTRODUCTION

Microporous semicrystalline membranes of controlled pore size, shape and distribution can be prepared by a process called thermally-induced phase separation (TIPS) as described in the first two papers in this series[1,2] and elsewhere[3-19]. In isothermal TIPS, the temperature at which TIPS occurs and the diluent concentration affect the rate at which TIPS occurs and, therefore, significantly influence the membrane structure and properties. The polymer–diluent system reported here undergoes solid–liquid TIPS as the polymer crystallizes. The objective of this study was to understand how the crystallization temperature (T_c) and the presence of diluent affect the polymer crystallization kinetics and the resulting solid-phase morphology.

Few studies of polymer crystallization from mixtures with low-molecular-weight diluents over wide concentration ranges have appeared in the literature. Most of these studies have concentrated on developing crystallization kinetics equations[20,21] and describing the effect of dilution on the polymer crystallization rate and crystal morphology[22]. Keith and Padden[23,24] proposed that diluent addition reduces polymer nucleation density and increases polymer mobility. Consequently, crystallization rate and spherulite morphology were significantly changed when iPP crystallized in the presence of low-molecular-weight atactic polypropylene[23-25].

MATERIALS AND METHODS

Materials

Himont X8773-66-6 isotactic polypropylene, iPP, was supplied by Dr Dziemianowicz of the Himont research centre. The iPP is a reactor-grade flake with intrinsic viscosity of approximately four. The molecular weight of the untreated iPP sample was determined by high-temperature gel permeation chromatography to be $M_n = 4.24 \times 10^4$ and $M_w = 3.01 \times 10^5$. Dotriacontane, $C_{32}H_{66}$, was obtained from Alfa Chemicals with a guaranteed purity up to 99.9% and a melting point of 342.9 K.

Sample preparation

iPP and $C_{32}H_{66}$ were weighed (total weight varied from 0.5 to 2 g depending on the diluent concentration required) and mixed with 100 ml of *p*-xylene in a 250 ml flask. The *p*-xylene had been filtered through a 0.2 μm Millipore Corp. Fluoropak filter prior to use. The mixture was purged with nitrogen for 15 min and then boiled with agitation under a nitrogen purge for 30 min. The polymer and diluent were crystallized as a homogeneous blend by pouring the hot solution into liquid nitrogen. To extract any *p*-xylene trapped in the solid sample, the liquid nitrogen plus *p*-xylene containing the iPP–$C_{32}H_{66}$ solid blend was washed in methanol that had been filtered with a 0.2 μm regenerated cellulose filter. The methanol suspension was filtered again, and the iPP–$C_{32}H_{66}$ blend recovered and dried at room temperature in a vacuum oven for at least 2 days until a constant weight was obtained. *FT*i.r. results showed no residual *p*-xylene in the sample. The resulting loosely-packed flakes were formed into a thin film by placing the sample between aluminium foil sheets and compression plates and applying 6890 kPa (1000 psi) pressure in a WABASH hydraulic compression moulder for 5 min. Samples taken from various points in the film and analysed on the differential scanning calorimeter, d.s.c., showed melting point repeatability of ± 0.1 K.

* Current address: Exxon Chemical Company, Baytown, TX 77522–5200, USA
† To whom correspondence should be addressed

0032–3861/93/224740–07

Table 1 Crystallization temperature range investigated

iPP (wt%)	T_c range (K)
100	403–415
90	401–408
80	398–405
70	395–403
60	394–402
50	390–397
40	387–395
30	385–393
20	381–389
10	380–386

Sample analysis

The kinetic studies were conducted on a Perkin–Elmer DSC7. The kinetics of iPP–$C_{32}H_{66}$ systems were investigated for mixtures with iPP concentrations ranging from 10 to 100 wt% at 10 wt% intervals. Each sample was sealed in an aluminium sample pan and heated in the d.s.c. to 473 K. Preliminary experiments indicated that 10 min at 473 K make the half-time reproducible. After heating, the sample was quenched at the fastest rate possible in the DSC7 to obtain the desired crystallization temperature and the thermogram was recorded. The melting point was determined by annealing the sample at a specified T_c for 6 h and then heating at 10 K min^{-1}. The melting peak temperature was taken as the melting point for a specified T_c.

Data analysis

Calorimetry was used to measure the heat liberated during crystallization as an indication of the overall crystallization rate[26]. The measured relative crystallinity, X, defined as the ratio of crystallinity developed at time t to crystallinity developed at $t \to \infty$, can be correlated by the Avrami equation[27–29]:

$$1 - X = \exp(-Kt^n) \quad (1)$$

X is experimentally obtained as

$$X = Q_t/Q_0 \quad (2)$$

where

K is the crystallization constant (min^{-n}),

t is the time elapsed (min),

n is the Avrami exponent, indicative of possible spherulitic morphologies and nucleation mechanisms[29] (dimensionless),

Q_t is the total heat evolved at time t (mW),

Q_0 is the total heat evolved as time approaches infinity (mW), and

X is the relative crystallinity (dimensionless).

Equation (1) can be transformed into

$$\ln\{-\ln(1-X)\} = n \ln t + \ln K \quad (3)$$

A plot of $\ln\{-\ln(1-X)\}$ *versus* $\ln t$ should yield a straight line with slope n and intercept $\ln K$ if the Avrami theory applies.

RESULTS AND DISCUSSION

Crystallization temperatures used in the kinetics experiments are listed in *Table 1*.

Effect of T_c *and dilution on crystallization mechanism*

Typical crystallization isotherms are shown in *Figure 1*. Isotherms for the 60 and 20 wt% iPP samples exhibited behaviour similar to the diluted systems shown in *Figure 1*. For 100 wt% iPP, the Avrami plot is a straight

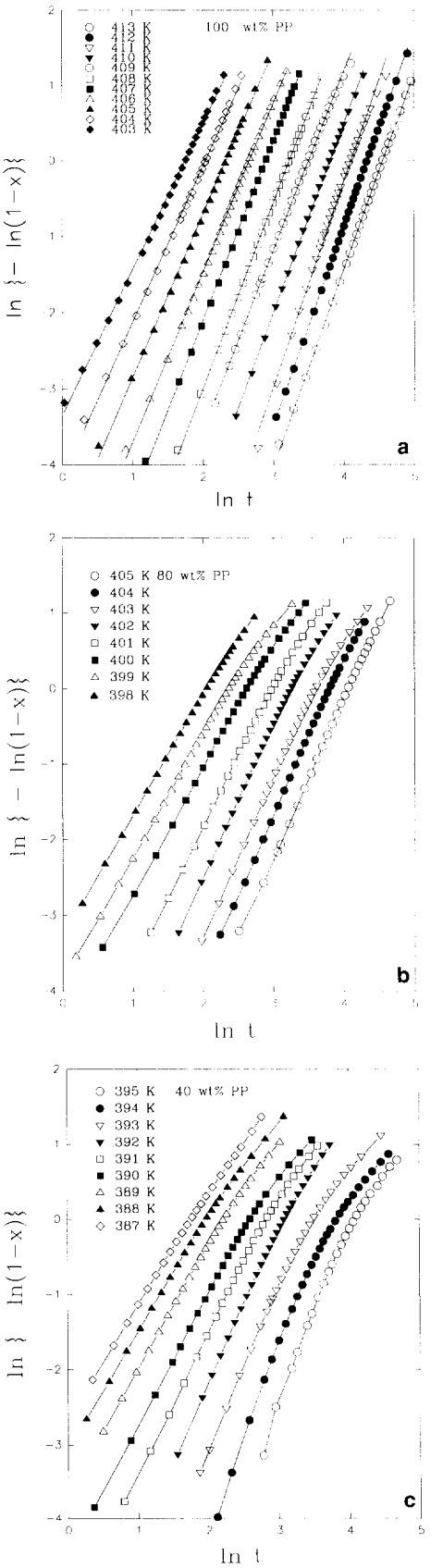

Figure 1 Crystallization isotherms of (a) pure iPP (413–403 K), (b) 80 wt% iPP (405–398 K), and (c) 40 wt% iPP (395–387 K)

line up to 90% relative crystallinity, while the lines are non-linear when the relative crystallinity is greater than 60% ($\ln\{-\ln(1-X)\} = -0.08$) for diluted samples. This non-linear behaviour has been observed in iPP[30] as well as in other pure polymer and polymer–diluent systems and attributed to 'secondary crystallization'[31–36]. After primary crystallization (0 to 60% crystallinity) or crystallization times longer than twice the half-time[37], slower, secondary crystallization perfects the structure of the already-crystallized phase and further crystallizes some of the amorphous macromolecules. The perfection of crystallites follows an empirical logarithm law with time (that is, the fold period of crystallites or crystallinity increases with time logarithmically, and the rate increases with T_c)[29,38]. Molten polymer mobility is important in determining the secondary crystallization rate. Since the addition of diluent increases polymer mobility, the secondary crystallization effect is enhanced. Thus, secondary crystallization may have contributed to the earlier and more evident non-linear behaviour when iPP concentration is 80 wt% or lower. Other factors may have contributed to the non-linearity, as suggested in the following paragraphs.

Macromolecules are known to fractionate during crystallization[25,39]; that is, macromolecules of smaller molecular weight are rejected from the growth front. The rejected molecules accumulate between spherulites or within spherulites in inter-lamellar regions, depending on the crystallization kinetics. These short-chain macromolecules have a lower equilibrium melting temperature (T_m°). At a fixed T_c, the supercooling is less for the shorter-chain molecular weights than it is for the long-chain molecules. Thus, crystallization of the short chains occurs at a slower rate. The iPP used in this study has a polydispersity of 6.8. Thus, the blends of iPP and $C_{32}H_{66}$ of various concentrations should exhibit molecular fractionation to a greater extent as the polymer concentration decreases and T_c increases.

The rejection and accumulation of diluent at the amorphous–crystal interface may have also contributed to the deviation from linearity in the latter stages of crystallization. The iPP concentration of the mixture at the amorphous–crystalline interface decreases as the diluent is rejected by the growing spherulite. As the concentration of the available amorphous material is depleted, the diffusion of polymer segments to the amorphous–crystalline interface can become rate-determining[40]. If this is the case, the spherulite growth rate and overall crystallization kinetics become non-linear.

Finally, the accumulation of the diluent between the spherulites may have physically retarded the growth of the spherulites, as suggested by Mandelkern[20]. As two spherulites approach each other, the volume-filling diluent acts as a physical restraint to the growing spherulites. For pure iPP, the retardation is not so evident, but the magnitude of the effect increases with increasing initial diluent concentration.

Effect of T_c *and dilution on the Avrami exponent*

The slope of lines in *Figure 1* were determined as follows:

(i) A likely break point where the line began to deviate from a straight line was selected based on visual inspection.

(ii) Regression analysis was performed using the selected break point and the end point to the left of the selected break point.

(iii) The end point in (ii) was omitted and the regression was repeated.

(iv) Step (iii) was repeated until the number of points between the break point and the new end point was equal to four points.

(v) The analysis in (ii) to (iv) was repeated with a new break point, which was situated five points to the left of the previous break point.

(vi) The group of points that yielded the best regression correlation coefficient was selected and the slope was determined.

Table 2 lists the Avrami exponents for various concentrations and T_c. Assignment of morphology to specific values of the Avrami exponent has been attempted in the literature, based on the result of studies conducted using pure polymer melts. Non-integral Avrami exponents have been observed in almost all polymer systems studied[41–44]. Banks and Sharples[45] and Sharples and Swinton[46] attributed fractional Avrami exponents to the decreasing average density within the growing spherulite with crystallization time. Hillier[30] attributed the non-integral exponent to the impingement of spherulites. Wunderlich[29] has attributed an exponent

Table 2 Effect of T_c and dilution on the Avrami exponent n (95% confidence limits given where available)

T_c (K)	iPP/C_{32}/H_{66} (weight ratio)				
	100/0	90/10	80/20	70/30	60/40
413	2.7				
412	2.6				
411	2.6±0.0				
410	2.6±0.0				
409	2.5±0.1				
408	2.5±0.1	2.5			
407	2.4±0.0	2.3±0.0			
406	2.3±0.0	2.2±0.0			
405	2.2±0.1	2.2±0.1	2.1±0.1		
404	2.0±0.0	2.1±0.2	2.1±0.1		
403	1.9±0.0	2.0±0.1	2.1±0.1	2.5	
402		1.9±0.2	2.0±0.3	2.2±0.0	2.3
401		1.7±0.1	1.9±0.1	2.2±0.2	2.2±0.3
400			1.7±0.1	2.1±0.0	2.2±0.2
399			1.6±0.1	2.0±0.2	2.1±0.0
398			1.5±0.2	1.9±0.2	1.9±0.0
397				1.7±0.3	1.8±0.2
396				1.6±0.2	1.7±0.3
395				1.5±0.2	1.5±0.1
394					1.4±0.1
	50/50	40/60	30/70	20/80	10/90
397	2.3				
396	2.1±0.1				
395	2.0±0.0	2.4			
394	1.8±0.1	2.3±0.1			
393	1.7±0.1	2.2±0.1	1.9±0.2		
392	1.7±0.0	2.1±0.1	1.9±0.2		
391	1.5±0.1	1.9±0.0	1.8±0.1		
390	1.5±0.1	1.8±0.1	1.8±0.1		
389		1.6±0.1	1.8±0.0	1.9	
388		1.6±0.0	1.6±0.0	1.9±0.1	
387		15.±0.0	1.5±0.1	1.9±0.0	
386			1.4±0.0	1.8±0.0	1.9±0.1
385			1.4±0.1	1.7±0.0	1.8±0.1
384				1.6±0.1	1.7±0.2
383				1.5±0.1	1.6±0.1
382				1.3±0.1	1.5±0.1
381					1.5±0.1
380					1.4±0.1

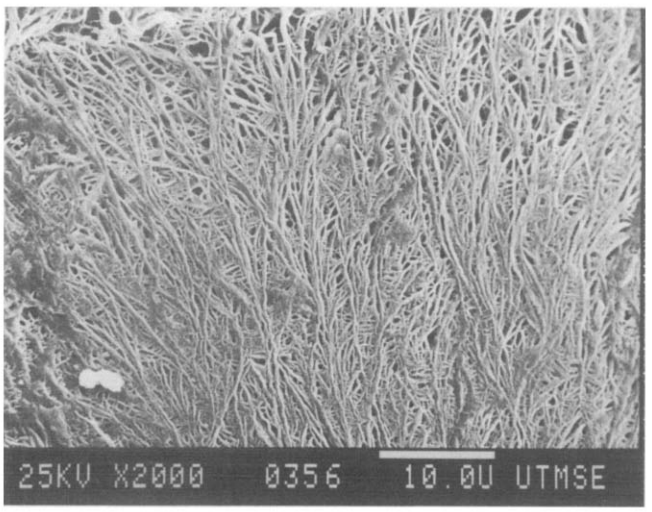

Figure 2 Scanning electron micrograph of iPP crystallized at 493 K (30 wt% iPP in $C_{32}H_{66}$)

of 3 to spherical structure resulting from instantaneous nucleation (that is, the number of nuclei, N, reaches a steady value rapidly after crystallization begins) and an exponent between 2 and 3 to truncated spheres resulting from instantaneous nucleation. Wunderlich[29] has attributed an exponent of 1.5 to spherical structure resulting from instantaneous nucleation with diffusion control.

Table 2 shows that as T_c decreases for a given iPP concentration, the exponent n decreases. The Avrami exponent of pure iPP is close to 3 at higher T_c, indicating that the nucleation is instantaneous. This is expected since sporadic nucleation is rarely observed unless the sample is free of all foreign material (such as catalyst or dust)[47]. As T_c decreases, the nucleation density increases. Since more spherulites are initiated per unit volume at lower T_c, spherulite truncation from impingement prevents the spherulites from developing a fully three-dimensional morphology. The Avrami exponent of nearly 2 for pure iPP at lower T_c appears to confirm this hypothesis.

For a given T_c, the exponent increases as the iPP concentration in the sample decreases since the nucleation density decreases and there is less spherulite truncation.

Effect of diluent rejection on the Avrami exponent

Electron microscopy[48] has shown that spherulite morphology is characterized by parallel-packed lamellae clusters separated by voids for the 30 and 10 wt% iPP systems crystallized at the supercoolings in this study (see *Figure 2*). The spherulite structure is described as 'open' or 'fibrillar'[25]. The lamellae in an 'open' spherulite grow more independent of each other than they do in the compact spherulites Wunderlich[29] used to relate spherulite structure and Avrami exponent.

The diluent is rejected from the spherulite during crystallization and accumulated at the growth front. The diluent accumulation is most pronounced when the crystallization rate is fast, since the diffusion mechanism does not have time to reduce the concentration gradient. Thus, at lower T_c, which has a fast crystallization rate, the spherulite radius is not proportional to t as in the derivation of equation (1), but rather to $t^{1/2}$ [25,29] and the exponent of t in equation (1) will be 1.5 rather than 3. This behaviour has been observed in the optical microscopy study and mathematical modelling of the iPP–$C_{32}H_{66}$ system[48,49]. The Avrami exponent should also decrease from the value of 3 predicted by equation (1) as the iPP concentration in the system decreases. For systems crystallized at low T_c, the Avrami exponent should decrease as the iPP concentration decreases since both lower T_c and lower polymer concentration enhance diluent accumulation at the growth front. *Table 2* shows that the Avrami exponent is below 2 at low T_c in 30 to 10 wt% iPP systems.

In summary, the Avrami exponent for high polymer concentration systems may be controlled by the three-dimensional spherulite morphology at high T_c and by spherulite truncation at lower T_c. For lower iPP concentration systems at lower T_c the Avrami exponent may be determined by a combination of diluent rejection at the inter-spherulite boundary and its inclusion within the spherulite.

Effect of T_c and dilution on crystallization rate

Figure 3 shows the effect of dilution on the time required for 50% of the crystallizable iPP to crystallize, $t_{1/2}$. The $t_{1/2}$ values are accurate to within $\pm 5\%$. $t_{1/2}$ is a measure of crystallization rate at a given temperature; the greater $t_{1/2}$, the slower the crystallization. *Figure 3* shows $t_{1/2}$ increases exponentially with increasing T_c in the T_c range explored when the concentration of the system remains constant. $t_{1/2}$ also decreases with increasing iPP concentration at a constant T_c.

Figure 4 shows $t_{1/2}$ of various concentrations at constant ΔT, where the supercooling was calculated as described below. In *Figure 4*, the crystallization half-time increases with increasing iPP concentration, reaches a maximum in the neighbourhood of 80 wt% iPP, and then decreases as iPP concentration increases. Since the thermodynamic driving force is the same at constant supercooling, kinetic factors must be considered to explain the maximum half-time in *Figure 4*.

The half-time can be correlated with $1/T_c\Delta Tf$[32,50]:

$$\ln(1/t_{1/2}) + U^*/R(T_c - T_\infty) = \ln G_0 - K_g/T_c\Delta Tf \quad (4)$$

or in an alternate form

$$\ln(1/t_{1/2}) + U^*/R(T_c - T_\infty) = \ln G_0 - (K_g/T_m^\circ)(T_m^\circ/T_c\Delta Tf) \quad (4a)$$

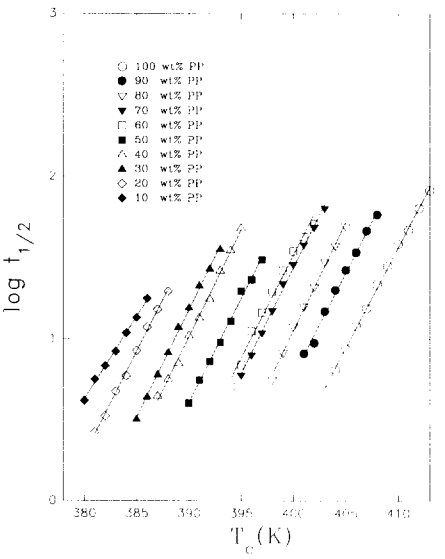

Figure 3 Effect of iPP concentration on $t_{1/2}$ as a function of T_c

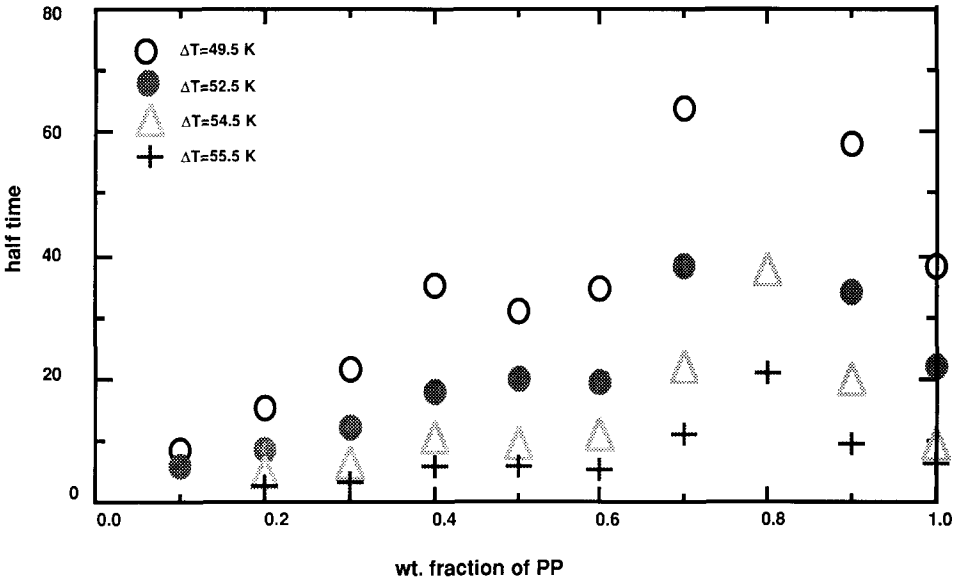

Figure 4 Effect of iPP concentration on $t_{1/2}$ as a function of ΔT

Table 3 Effect of iPP concentration on T_m° and kinetic parameters (95% confidence limits given where available)

iPP (wt%)	T_m° (K)	$T_m^\circ - T_g$ (K)	K_g $\times 10^{-5}$ (K^2)	ln G_0	σ_e (erg cm^{-2})
100	459.5±2.5	200.5	4.22±0.18	22.4±0.8	86.1±3.6
90	457.8±2.1	219.9	4.19±0.15	21.4±0.7	85.8±3.0
80	455.4±3.3	236.0	4.12±0.37	20.8±1.8	84.8±7.6
70	452.6±2.7	248.1	3.87±0.33	19.7±1.6	80.2±6.7
60	449.7±4.2	258.6	3.99±0.23	20.9±1.2	83.1±4.8
50	447.0±1.0	267.6	3.81±0.12	19.8±0.6	79.8±2.4
40	444.2±1.4	276.2	3.84±0.26	19.9±1.4	80.9±5.6
30	440.3±1.8	280.6	3.67±0.17	20.0±0.6	78.1±3.5
20	436.3±2.0	284.8	3.59±0.34	19.9±1.8	77.0±7.3
10	432.4±2.9	288.4	3.04±0.34	17.7±2.0	65.9±7.5

As reported elsewhere[48] the experimental data fall into regime III kinetics; consequently, K_g is defined for regime III as

$$K_g = 4b\sigma\sigma_e T_m^\circ / k\Delta H \quad (5)$$

where

σ_e is the fold surface free energy (erg cm^{-2}),
σ is the lateral surface free energy (erg cm^{-2}),
G_0 is the pre-exponential factor (dimensionless),
ΔH is the polymer heat of fusion (erg cm^{-3}),
k is the Boltzmann constant (erg K^{-1} mol^{-1}),
T_c is the polymer crystallization temperature (K),
T_∞ is the temperature at which polymer crystallization ceases (K),
T_m° is the equilibrium melting temperature (K),
ΔT is the degree of supercooling, defined as $T_m^\circ - T_c$ (K),
U^* is the Williams, Landel and Ferry (WLF) shift constant (kcal mol^{-1}),
R is the gas constant (kcal mol^{-1} K^{-1}) and
f is defined by $2T_c/(T_m^\circ + T_c)$.

Hoffman *et al.*[36] found $T_\infty = T_g - 30$ K and $U^* = 1500$ cal mol^{-1} by fitting the crystallization kinetics rate data for various polymers with equation (3). In this work, a value for T_g was estimated using the Fox equation[51]:

$$1/T_{g(mix.)} = W_{PP}/T_{g(PP)} + W_{C32}/T_{g(C32)} \quad (6)$$

where W_i and T_{gi} are the mass fraction and the glass transition temperature of component i. T_g of dotriacontane was estimated to be 137.2 K using the equation developed by Fedors[52,53]. A value of $T_g = 259$ K was used for iPP[54].

The approach suggested by Hoffman and Weeks[55] was adopted in this study to determine the equilibrium melting temperature. The equilibrium melting points obtained by this method are listed in *Table 3*. T_m° of pure iPP was determined to be 459.5 K by the Hoffman–Weeks method using experimental T_c between 380 and 403 K. The T_m° is comparable to 459 K obtained by Krigbaum and Uematsu[56] and 457 K by Danusso and Gianotti[57].

Effect of mobility term on crystallization rate at constant ΔT

The polymer crystallization rate is controlled by two factors: nucleation rate and polymer mobility. In equation (4), the mobility term $U^*/R(T_c - T_\infty)$ accounts for the effect of viscosity on the transport of polymer molecules from the amorphous phase to the crystal phase. The polymer mobility increases with increasing $(T_c - T_\infty)$. By substituting for T_∞, it can be shown that

$$T_c - T_\infty = T_c - T_g + 30 = (T_m^\circ - T_g) - (T_m^\circ - T_c) + 30$$
$$= (T_m^\circ - T_g) - \Delta T + 30 \quad (7)$$

From *Table 3*, $(T_m^\circ - T_g)$ increases with decreasing polymer concentration. Thus, polymer mobility increases with decreasing polymer concentration. The increased polymer mobility may increase the crystallization rate by increasing the rate that the molecules can move to the crystalline–amorphous interface to crystallize.

Effect of nucleation rate on crystallization rate at constant ΔT

In equation (4), the nucleation term $-K_g/T_c\Delta Tf$ accounts for the secondary nucleation barrier of polymer molecules[36]. For homopolymers, the nucleation rate increases with decreasing T_c, thus the crystallization rate increases with decreasing T_c. However, polymer mobility decreases as T_c is decreased. Thus, a maximum crystallization rate is observed. A maximum in growth

rate as a function of T_c has been reported for systems of isotactic polystyrene[58] and Nylon 6[59]. Thus, the maximum in crystallization rate observed in *Figure 4* may be caused by the opposing effects on nucleation rate and polymer mobility.

Equation (4) shows that at constant ΔT, T_c ($= T_m^\circ - \Delta T$) decreases with increasing diluent concentration (that is, decreasing iPP concentration) due to T_m° depression. Thus, the nucleation rate decreases and polymer mobility increases as polymer concentration decreases at the same supercooling. Consequently, as the initial iPP concentration is decreased from 100 to 70 wt% the crystallization rate decreases because the crystallization rate is dominated by the nucleation rate. Further decreases in polymer concentration enhances the crystallization rate since polymer mobility increases to override the decreasing nucleation rate.

Effect of T_c *and dilution on fold surface energy*

Figure 5 shows the plot of equation (4a) for various iPP concentrations. $t_{1/2}$ and the corresponding $1/T_c\Delta Tf$ of each polymer concentration were analysed using equation (4). The slope and intercept of the lines obtained from equation (4) are listed in *Table 3*. *Table 3* implies that the intercept $\ln G_0$ shows no significant trend with concentration.

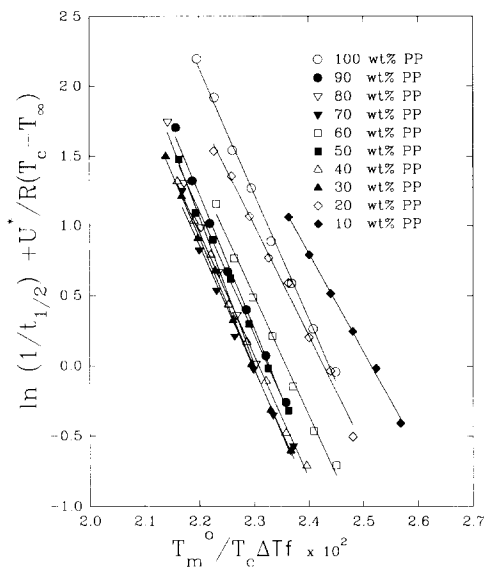

Figure 5 Plots of equation (4a) for iPP–$C_{32}H_{66}$ system at various concentrations

The K_g values obtained from $t_{1/2}$ were analysed using equation (4). The slope of equation (4) yielded the fold surface energy, σ_e, using equation (6). For iPP, $a \times b = 34.37$ Å^2, $b = 6.26$ Å on the (110) growth plane, $\sigma = 11.5$ erg cm^{-2}, length of monomer unit = 2.165 Å, and $\Delta H = 1.96 \times 10^9$ erg cm^{-3} [60]. The side surface free energy has been assumed a material constant and independent of diluent or polymer concentration (in the case of polymer blends system) in nearly all crystallization kinetic data analysis. This assumption is correct if there are few diluent molecules or no diluent molecules included in the crystal. Thus, the crystallizing polymers see minimum diluent (concentration) effect while depositing on the growth surface of the substrate. This is also discussed in ref. 48.

Some error may have been introduced by assuming the growth is only on the (110) plane. It has been shown that more than one growth plane is involved in regime III growth[60,61]. However, ref. 60 also indicates that the experimental value of K_g in regime III is nearly twice that of K_g in regime II, implying that the error is small when assuming the growth plane is only (110). This has been verified for the kinetic data[48]. Additional evidence for this assumption comes from the work of Wittman and Lotz[62,63], who show PE molecules crystallize epitaxially with PP. The crystal growth plane is not altered by the presence of PE. Since dotriacontane is an analogue of PE, it is reasonable to assume the iPP growth plane is not altered in this case.

The fold surface energy listed in *Table 3* appears to decrease slightly as the polymer concentration decreases from 100 wt%. Further research is required to confirm the behaviour in σ_e.

Comparison of kinetic data with literature data

The three major methods involving Avrami analysis of crystallization kinetics data include polarized light microscopy, dilatometry and d.s.c. A comparison of kinetic data obtained by different scientists is difficult not only because they used different instruments, but also because the methods and parameters used to analyse the data varied.

Slonimsky and Godovsky found the Avrami exponents obtained from calorimetry and dilatometry do not agree[64] because of the different measuring principles of the two methods[65]. Calorimetry measures the growth of lamellae, which are the finer forms of macromolecular structure. Dilatometry registers changes in spherulite structure, which depends on lamellae packing within the

Table 4 Comparison of K_g from the literature

Data source	K_g $\times 10^{-5}$ (K^2)	σ_e (erg cm^{-2})	Method	Sample preparation
Monasse and Haudin[67a]	5.96	121	Microscopy	483 K, 5 min
Martuscelli *et al.*[67]	5.02	102	Calorimetry	≈473 K, 10 min
This study	4.22	86.1	Calorimetry	493 K, 10 min
Binsbergen[60]	3.61	74.2	Dilatometry	483 K, 15 min
Keith and Padden[60]	3.34	68.7	Microscopy	473 K
Godovsky and Slonimsky[69]	3.22	65.7	Calorimetry	463 K, 10 min
Falkai and Stuart[60]	3.18	65.4	Microscopy	453 K, 15 min
Wang and Lloyd[70]	2.78	56.7	Microscopy	493 K, 10 min
Lim and Lloyd[1]	3.92	91.8	Calorimetry	493 K, 10 min

[a] Clark and Hoffman[60] used $\Delta H = 1.96 \times 10^9$ erg cm^{-2} to calculate σ_e, while Monasse and Haudin[67] used 1.4×10^9 erg cm^{-2}. The actual K_g value in ref. 67 is 7.28×10^5 (K^2)

spherulite[64], and is on a larger scale than the lamellae formation.

Another factor that makes comparison of kinetic data difficult is the different molecular weights used by many investigators. Different molecular weights cause differences in the crystallization rate[66], and thus in the half-times. This makes the comparison of iPP half-times with other studies not practical. However, σ_e should be the same for pure iPP since it reflects the work of chain folding and is independent of the iPP used. Comparison of K_g for pure iPP reveals that differences in measurement techniques, sample preparation and molecular weight can lead to a difference in K_g. *Table 4*, which lists K_g from the literature, shows considerable scatter. Even K_g values from the same method do not agree with each other. The σ_e obtained from calorimetry is higher than those obtained from microscopy and dilatometry, with the exception of Godovsky and Slonimsky's data. Again, differences can be attributed to differences in the quantities measured by different instruments. Calorimetry measures the overall crystallization rate which involves all spherulites crystallized in the system and nuclei formation. Microscopy measures the radius of a single spherulite.

CONCLUSIONS

Calorimetry has been used to study the effect of diluent addition on iPP crystallization rate and morphology. Diluent addition increases the crystallization rate most likely by enhancing polymer ability to disentangle in the melt, move to the amorphous–crystalline interface, and deposit on the growing crystal. The diluent rejection at the growth front affects the lamellae morphology and the growth rate as reflected by the change in the Avrami exponent. The fold surface energy was found to decrease slightly as the polymer concentration decreases from 100 wt%, eventually reaching a constant value at the lower polymer concentrations.

ACKNOWLEDGEMENTS

The authors gratefully acknowledge the continued generous financial support of the Texas Advanced Technology Program and the Central Research Technology Development Laboratory of the 3M Company, St. Paul, MN. The authors also thank Dr A. J. Peacock for helpful discussions.

REFERENCES

1 Lim, G. B. A. and Lloyd, D. R. *Polym. Eng. Sci.* 1993, **33**, 522
2 Lim, G. B. A. and Lloyd. D. R. *Polym. Eng. Sci.* 1993, **33**, 513
3 Hiatt, W. C., Vitzthum, G. H., Wagener, K. B., Gerlach, K. and Josefiak, C. in 'Materials Science of Synthetic Membranes' (Ed. D. R. Lloyd), ACS Symposium Series 269, American Chemical Society, Washington, DC, 1985
4 Caneba, G. T. and Soong, D. S. *Macromolecules* 1985, **18**, 2538
5 Caneba, G. T. and Soong, D. S. *Macromolecules* 1985, **18**, 2545
6 Lloyd, D. R., Barlow, J. W. and Kinzer, K. E. in 'New Membrane Materials and Processes for Separation' (Eds K. K. Sirkar and D. R. Lloyd), AIChE Symposium Series 261, American Institute of Chemical Engineers, New York, NY, 1988
7 Lloyd, D. R., Kinzer, K. E. and Tseng, H. S. *J. Membr. Sci.* 1990, **52**, 239
8 Lloyd, D. R., Kim, S. S. and Kinzer, K. E. *J. Membr. Sci.* 1991, **64**, 1
9 Kim, S. S. and Lloyd, D. R. *J. Membr. Sci.* 1991, **64**, 13
10 Lim, G. B. A., Kim, S. S., Ye, Q. H., Wang, Y. F. and Lloyd, D. R. *J. Membr. Sci.* 1991, **64**, 31
11 Kim, S. S., Lim, G. B. A., Alwattari, A. A., Wang, Y. F. and Lloyd, D. R. *J. Membr. Sci.* 1991, **64**, 41
12 Alwattari, A. A. and Lloyd, D. R. *J. Membr. Sci.* 1991, **64**, 55
13 McGuire, K. S., Lloyd, D. R. and Lim, G. B. A. *J. Membr. Sci.* 1993, **79**, 27
14 Castro, A. J. *US Patent 4 247 498*, 1981
15 Vitzthum, G. H. and Davis, M. A. *US Patent 4 490 431*, 1984
16 Shipman, G. H. *US Patent 4 539 256*, 1985
17 Mrozinski, J. S. *US Patent 4 726 989*, 1988
18 Kinzer, K. E. *US Patent 4 867 881*, 1989
19 Lopatin, G., Yen, L. and Rogers, R. R. *European Patent Application 88 106 209.5*, 1988
20 Mandelkern, L. *J. Appl. Phys.* 1955, **26**, 443
21 Boon, J. and Azcue, J. M. *J. Polym. Sci.* 1968, **6**, 885
22 Chaturvedi, P. N. *Makromol. Chem.* 1987, **188**, 433
23 Keith, H. D. and Padden, F. J. *J. Appl. Phys.* 1964, **35**, 1270
24 Keith, H. D. and Padden, F. J. *J. Appl. Phys.* 1964, **35**, 1286
25 Keith, H. D. and Padden, F. J. *J. Appl. Phys.* 1963, **34**, 2409
26 Cimmino, S., Martuscelli, E., Silvestre, C., Canetti, M., de Lalla, C. and Seves, A. *J. Polym. Sci., Polym. Phys. Edn* 1989, **27**, 1781
27 Avrami, M. *J. Chem. Phys.* 1939, **7**, 1103
28 Avrami, M. *J. Chem. Phys.* 1940, **8**, 212
29 Wunderlich, B. 'Macromolecular Physics', Vol. 2, Academic Press, New York, 1976, Ch. 6
30 Hillier, I. H. *J. Polym. Sci., Polym. Phys. Edn* 1966, **4**, 1
31 Hay, N. J. and Booth, A. *Polymer* 1969, **10**, 95
32 Phillips, P. J. and Kao, Y. H. *Polymer* 1986, **27**, 1679
33 Devoy, C., Mandelkern, L. and Bourland, L. *J. Polym. Sci., Polym. Phys. Edn* 1970, **8**, 869
34 Chynoweth, K. R. and Stachurski, Z. H. *Polymer* 1986, **27**, 1912
35 Cebe, P. and Hong, S. *Polymer* 1986, **27**, 1183
36 Hoffman, J. D., Davis, G. T. and Lauritzen, J. I. in 'Treatise on Solid State Chemistry' (Ed. N. B. Hannay), Plenum Press, New York, 1976
37 Rybnikar, F. *J. Polym. Sci., Polym. Phys. Edn* 1963, **1**, 2031
38 Carfagna, C., De Rosa, C., Guerra, G. and Petraccone, V. *Polymer* 1984, **25**, 1462
39 Wunderlich, B. and Mehta, A. *J. Polym. Sci.* 1974, **12**, 255
40 Asaubekov, M. A., Krasnikova, N. P. and Kargin, V. A. *Vysokomol. Soedin., Ser. A* 1972, **14** (1), 30
41 Russell, G. S. F. and Pillai, P. S. *Makromol. Chem.* 1970, **135**, 263
42 Mancarella, C. and Martuscelli, E. *Polymer* 1977, **18**, 1240
43 Vilanova, P. C., Ribas, S. M. and Guzman, G. M. *Polymer* 1976, **17**, 423
44 Lopez, L. C. and Wilkes, G. L. *Polymer* 1988, **29**, 106
45 Banks, W. and Sharples, A. *Makromol. Chem.* 1963, **59**, 233
46 Sharples, A. and Swinton, F. L. *Polymer* 1962, **6**, 119
47 Ross, G. S. and Frolen, L. J. in 'Methods of Experimental Physics' (Ed. R. A. Fava), Academic Press, New York, 1980
48 Wang, Y. F. and Lloyd, D. R. *Polymer* to be submitted
49 Wang, Y. F. and Lloyd, D. R. *Polymer* to be submitted
50 Godovsky, Y. K. and Shibanov, Y. D. *Polym. Sci. USSR* 1982, **24**, 1116
51 Paul, D. R. and Newman, S. 'Polymer Blends', Academic Press, New York, 1978
52 Fedors, R. F. *Polym. Commun.* 1979, **20**, 1055
53 Fedors, R. F. *Polymer* 1979, **20**, 1255
54 Plazek, D. L. and Plazek, D. J. *Macromolecules* 1983, **16**, 1469
55 Hoffman, J. D. and Weeks, J. J. *J. Res. Natl Bur. Stand, Sect. A* 1962, **66**, 13
56 Krigbaum, W. R. and Uematsu, I. *J. Polym. Sci., Part A* 1965, **3**, 767
57 Danusso, F. and Gianotti, G. *Makromol. Chem.* 1964, **80**, 1
58 Suzuki, T. and Kovacs, A. J. *Polymer* 1960, **1**, 82
59 Magill, J. H. *Polymer* 1962, **3**, 655
60 Clark, E. J. and Hoffman, J. D. *Macromolecules* 1984, **17**, 878
61 Guttman, C. M. and Dimarzio, E. A. *J. Appl. Phys.* 1983, **54**, 5541
62 Wittmann, J. C. and Lotz, B. *J. Polym. Sci., Polym. Phys. Edn* 1986, **24**, 1541
63 Wittmann, J. C. and Lotz, B. *J. Polym. Sci., Polym. Phys. Edn* 1986, **24**, 1559
64 Slonimsky, G. L. *J. Polym. Sci., Part C* 1970, **30**, 283
65 Godovsky, Y. K., Slonimsky, G. L. and Garbar, N. M. *J. Polym. Sci., Part C* 1972, **38**, 1
66 Fatou, J. M. G. and Riande, E. *Polymer* 1976, **17**, 99
67 Monasse, B. and Haudin, J. M. *Colloid Polym. Sci.* 1985, **263**, 822
68 Martuscelli, E., Pracella, M. and Crispino, L. *Polymer* 1983, **24**, 693
69 Godovsky, Y. K. and Slonimsky, G. L. *J. Polym. Sci., Polym. Phys. Edn* 1974, **12**, 1053
70 Wang, Y. F. and Lloyd, D. R. *Polymer* 1993, **34**, 2324